ACS OMEGA

Open Access

http://pubs.acs.org/journal/acsodf

Article

Exploring a Porous Biochar-Based Capacitive Deionization Device for Phosphogypsum Wastewater Treatment in Undergraduate Experimental Teaching: Understanding, Development, and Practice

Geming Wang,[#] Shiyu Zhou,[#] Ziheng Yang,[#] Dingdu Chen, Hongyang Zhao, Zhe Chen, Shuangfeng Hu, Sheikh Tamjidur Rahman,* and Qirui Wu*

Cite This: https://doi.org/10.1021/acsomega.5c05966

Read Online

ACCESS | Metrics & More | Article Recommendations | Supporting Information

ABSTRACT: Capacitive deionization (CDI) is a crucial technique for industries managing liquid chemical waste, requiring efficient electrode materials to ensure optimal performance. This study presents a novel undergraduate experimental teaching framework that integrates the understanding, development, and practical application of porous biochar-based CDI systems. Designed to support both students and educators, the curriculum guides learners through the synthesis of biochar electrodes via biomass pyrolysis and the assembly of CDI devices for treating phosphogypsum wastewater. Through material characterization and electrochemical analysis, students gain hands-on experience in electrode fabrication and CDI operation. The program concludes with student evaluations to assess the comprehension and skill development. By bridging materials science and chemical engineering, this interdisciplinary approach offers undergraduate students a comprehensive opportunity to translate their theoretical knowledge into practical solutions for sustainable wastewater treatment.

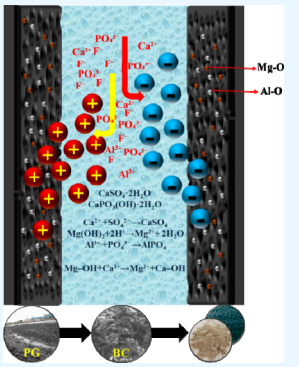

1. INTRODUCTION

Phosphogypsum is a byproduct of several industries, including fertilizer manufacturing (where gypsum-based fertilizers are produced) and chemical processing (where phosphoric acid is synthesized).[1,2] It poses significant environmental risks due to its content of radioactive elements, heavy metals, and toxic substances, which can leach into soil and groundwater.[3,2] Improper disposal further exacerbates environmental issues, leading to drainage blockages, dust pollution, and F release, underscoring the urgent need for sustainable management solutions.

To mitigate these risks, it is essential to treat the wastewater generated by these industries, which often contains phosphogypsum. While the primary component of phosphogypsum, $CaSO_4{\cdot}2H_2O$, is insoluble in water, contaminants such as F, P, and heavy metals can dissolve.[4] During the washing process, soluble phosphorus species ($H_2PO_4^-$, HPO_4^{2-}, PO_4^{3-}), F^-, and heavy metal ions leach into the water.[5]

Capacitive deionization[6] (CDI) is an emerging technology that reduces the cost of desalination and wastewater treatment compared to conventional methods like multieffect desalination,[7] reverse osmosis,[8] and multistage flash.[9] The process relies on creating an electrical imbalance between two electrodes immersed in an electrolyte. A standard CDI cell consists of two electrodes separated by an insulator, with an external voltage applied across them.[10] The resulting charge disparity, electron deficiency at the anode, and excess electrons at the cathode attract counterions that adsorb onto the electrode surfaces to restore charge balance. This electrosorption process continues until equilibrium is reached, forming an electrical double layer.[11]

Porous electrodes enhance ion storage capacity.[12,13] Once saturation occurs, removing the voltage triggers desorption, regenerating the electrodes for reuse.[14] Biomass-derived porous carbon materials are particularly promising for CDI due to their hierarchical pore structure (mesopores and micropores) and high surface area, which facilitate efficient ion adsorption.[15] Figure 1 illustrates the CDI process, which efficiently removes P and F ions from industrial wastewater via adsorption.

However, raw biochar typically exhibits limited adsorption capacity for specific contaminants like F and P. To address this limitation and enhance its applicability in CDI for phosphogypsum wastewater treatment, this study focuses on modifying biochar through activation with magnesium- and aluminum-based salts. Given the critical need for scalable and sustainable solutions to manage phosphogypsum pollution alongside the demand for training future environmental professionals in advanced remediation technologies, this

Received: June 25, 2025
Revised: August 1, 2025
Accepted: August 14, 2025

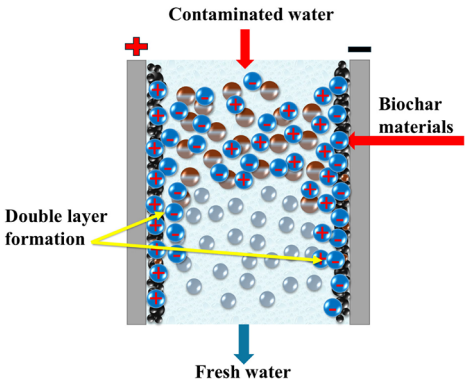

Figure 1. Schematic of the CDI process.

investigation adopts a pedagogical approach. We have designed a comprehensive hands-on experiment that guides university students through the entire process: from the preparation and activation of the biomass-derived carbon electrodes to the assembly, operation, and performance evaluation of a functional CDI system targeting F^- and soluble P species removal.

This study provides students with hands-on training in both biochar electrode preparation and the CDI system configuration for wastewater treatment. Through structured phases, including instrumentation familiarization and guided group discussions based on detailed protocols, participants gain direct experience in material synthesis, electrochemical system configuration, and analytical assessment of treatment efficiency. Given the scale of global industrialization, such practical knowledge is critical for conserving water resources and mitigating environmental harm. The experiment is divided into two phases: (1) instrument familiarization and (2) group discussions based on detailed handouts. To the best of our knowledge, no prior study has offered such a comprehensive, student-focused explanation of CDI experimental procedures. By bridging fundamental research with experiential learning, this study aims to advance both the technical understanding of CDI-based pollutant removal and the pedagogical tools available for cultivating skilled practitioners in sustainable water management.

2. LEARNING OBJECTIVES

The learning process is divided into two major modules: first, the preparation procedure of the biochar electrode and, second, the application of the electrode materials in the CDI device, along with a step-by-step guide for assembling the device.

The selection of biomass materials is the most crucial part of the first module. Students must understand how to choose an appropriate biomass based on its chemical composition, such as cellulosic content, lignin content, and origin, whether animal- or plant-based. Various types of waste, such as fruit peels, stems, seeds, or leaves, can be used as biomass materials, but their properties should be carefully considered for deeper understanding. Typically, materials with a high lignin content offer a better carbon yield and a more developed porous structure.

Processing the biomass for carbonization is another significant aspect of the experiment. Students should focus on the washing process, the chemicals involved, and whether the material should be ground into powder or cut into small pieces to improve the carbonization outcome. During the activation process, salt measurement based on the mass ratio is critical to prevent excessive salt use. This will help students appreciate the importance of resource optimization and teach them how to conduct experiments using only the necessary amounts of chemicals. Following activation, the next step is electrode preparation and proper storage of the extraporous biochar materials.

CDI technology directly addresses pressing issues related to hazardous waste disposal. These include the leaching of heavy metals into soil and water and the release of radioactive materials into the environment, all of which ultimately contaminate water sources. With industries continuously discharging wastewater containing toxic heavy metals into rivers and oceans, advanced electrodes in CDI devices can selectively remove these pollutants, thereby reducing aquatic pollution and protecting public health and safety.

In the case of phosphogypsum water washing effluents, the wastewater may contain high concentrations of P and F ions.[16] CDI technology can be applied to effectively separate and store these ions, allowing for their potential reuse in other applications. Through this process, students will learn not only the technical procedures but also the environmental risks associated with P and F in water. They will gain insights into the potential of CDI for environmental protection and the growing necessity of this technology for water purification efforts.

This learning process is divided into two modules: (1) biochar electrode preparation and (2) application of electrode materials in CDI devices, including a step-by-step guide for device assembly.

For module 1, students will learn to select appropriate biomass materials based on chemical composition (e.g., cellulose and lignin content) and origin (plant- or animal-based). They will evaluate different waste sources (fruit peels, stems, seeds, leaves) and understand how properties such as high lignin content improve carbon yield and porosity. Students will study pretreatment methods, including washing, grinding, or cutting biomass, to optimize carbonization. Emphasis will be placed on precise salt measurement (mass ratio) to avoid excess usage, teaching resource efficiency, and chemical optimization. Students will prepare biochar electrodes and learn proper storage techniques for porous biochar materials.

For module 2, students will explore how CDI addresses environmental challenges such as heavy metal leaching and radioactive contamination in water. They will examine how advanced CDI electrodes selectively remove toxic ions from industrial wastewater, mitigating water pollution, and protecting public health. Students will analyze CDI's role in treating phosphogypsum effluents, focusing on ion separation, recovery, and potential reuse.

During the lesson, the learning objectives can be outlined as follows:

Learn the principles of deionization

Understand the capacitive deionization process

Gain knowledge of biochar preparation and activation methods

Be familiar with the electrode material preparation from biochar

Identify the importance of deionization for water purification

https://doi.org/10.1021/acsomega.5c05966
ACS Omega XXXX, XXX, XXX−XXX

3. EXPERIMENTAL SECTION

3.1. Experimental Process. The experiment was conducted by 15 students, divided into three groups. Each group was assigned specific tasks and instructed to share their findings after each phase to foster collaborative learning. Prior to the experiment, students received a comprehensive handout containing: theoretical background (biochar chemistry, CDI principles, electrochemical testing), step-by-step experimental procedures, safety protocols, and descriptions of materials and reagents. Students were required to thoroughly review the Student's Handout, as it provided all background concepts, including biochar chemistry, CDI principles, and electrochemical testing.

After the completion of the practical steps, students underwent an oral assessment conducted by the instructor to evaluate their comprehension and ability to apply theoretical knowledge to practical problems. Tasks assigned to students included washing and grinding the biomass material, measuring and preparing chemical solutions, and processing the biomass into biochar under the supervision of the instructor. Following biochar synthesis, students participated in the activation process using magnesium chloride ($MgCl_2$) and aluminum chloride ($AlCl_3$) to enhance the surface properties of the biochar. The experimental protocol strictly adhered to the instructions provided in the handout, and students were expected to follow each step meticulously.

Upon completion of the biochar preparation and activation processes, students proceeded with the main experimental task of assembling and testing the CDI device following the operational guidelines. Students were encouraged to monitor key parameters and adapt the experimental conditions when necessary. For example, if the electrochemical characterization showed suboptimal specific capacitance, it would imply limitations in CDI performance. In such cases, students were instructed to reassess their procedures, adjust parameters such as temperature, salt ratio, or calcination duration, and repeat the experiment if required to optimize the results.

At the conclusion of the experiment, students were evaluated through a structured question-and-answer session. These assessment questions are documented in a later section. Instructors are encouraged to design a similar evaluation framework to assess students' conceptual understanding and practical competence.

3.2. Materials and Instruments. Coconut shells used for biochar production were collected from Hainan, China. These were initially washed with deionized water to remove surface impurities and oven-dried at 80 °C for 24 h. The dried shells were then ground into fine powder to ensure uniformity during carbonization. All chemical reagents, including $MgCl_2{\cdot}6H_2O$, $AlCl_3{\cdot}6H_2O$, and others used in the activation process, were sourced from Sinopharm Group Chemical Reagent Co. The carbonization of the biomass was conducted using a tube furnace (QSH-VTF, Shanghai Quansheo Electric Furnace Co., Ltd.). A standard ultrasonic cleaner was used for sample dispersion. Additional equipment included a grinder, a magnetic stirrer, and a vacuum filtration apparatus.

Characterization of the synthesized electrode materials was performed by using multiple analytical techniques. FESEM (ZEISS GeminiSEM 300) was used to observe the surface morphology. EDS was applied to determine the elemental distribution. X-ray diffraction (XRD, Bruker D8 Advance, Germany) was utilized to identify the crystal structure and phase composition. Raman spectroscopy (Thermo Fisher DXR) provided information about graphitic and disordered carbon structures. FTIR spectroscopy (Thermo Fisher Nicolet 6700) was used to detect functional groups in the range of 400−4000 cm^{-1}. XPS (Thermo Fisher ESCALAB XI+) enabled the analysis of surface chemistry before and after ion adsorption. Nitrogen adsorption−desorption isotherms were recorded using a fully automated gas sorption analyzer (Autosorb-iQ, Quantachrome). Surface area and pore size distribution were determined. Electrochemical measurements, such as cyclic voltammetry and electrochemical impedance spectroscopy, were performed using an electrochemical workstation (CHI 660E, Shanghai Chenghua Instruments Co., Ltd.).

3.3. Preparation of Biochar Materials. Initially, the cleaned coconut shell powder was oven-dried and then subjected to pyrolysis at 650 °C under a nitrogen (N_2) atmosphere for 2 h, yielding the biochar precursor (denoted as BC). This carbonization process converts the organic structure of the biomass into a porous carbon network by thermally decomposing volatile matter in an oxygen-limited environment. The BC product was washed with deionized water to remove residual ash or surface contaminants, dried at 60 °C, ground into fine powder, and sieved through a 50-mesh screen for uniformity and storage. Then, BC was mixed with $MgCl_2{\cdot}6H_2O$ in a 1:2 mass ratio in 100 mL of deionized water and stirred for 5 h using a magnetic stirrer to ensure uniform ion penetration into the porous structure. The mixture was oven-dried at 80 °C and subsequently calcined at 750 °C under a nitrogen atmosphere for 3 h. This step promotes activation by enhancing the porosity and doping magnesium into the carbon matrix. The resulting material, after being washed to remove residual salts, was labeled as Mg−BC. The Mg−BC and $AlCl_3$ were combined in a 1:2:2 mass ratio with 100 mL of water and stirred for 8 h. After drying at 80 °C, the codoped material was referred to as Mg−Al−BC. This codoping with aluminum further improves surface functionality, electrochemical properties, and ion selectivity due to enhanced surface polarity and functional group abundance. Finally, after the Mg−Al−BC adsorbed F and P ions during CDI testing, it was renamed Mg−Al−BC−F/P, indicating the presence of adsorbed P and F species.

It is critical to carefully control the pyrolysis temperature throughout this process. Too low a temperature (<300 °C) will result in incomplete carbonization and poor porosity, while excessively high temperatures (>700 °C) may lead to structural collapse or undesirable graphitization, which reduces ion-accessible surface area. The optimal range (650−750 °C) ensures a high degree of activation while maintaining sufficient pore volume for effective ion storage.

3.4. CDI Device Configuration. The capacitive deionization (CDI) unit consisted of four essential components: resin plates, silicon gaskets, titanium (Ti) electrodes, and biochar-based electrode material. A 1 mm-thick silicone separator was placed between the two Ti electrodes to prevent short-circuiting while allowing ion migration. These components were assembled into a sandwich structure held between two resin plates, forming a sealed CDI cell. A schematic of the CDI device is presented in Figure 2.

Activated biochar (Mg−Al−BC) was applied to the center of each titanium plate (10 × 10 cm) using a glass rod to ensure even coating. The coated Ti plates were dried in a vacuum

https://doi.org/10.1021/acsomega.5c05966
ACS Omega XXXX, XXX, XXX−XXX

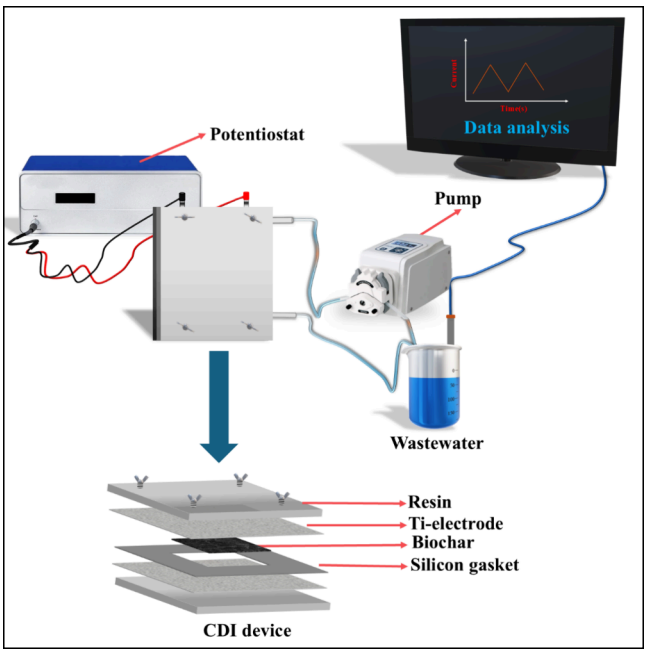

Figure 2. CDI unit assembly for the deionization process.

oven at 80 °C for 12 h to produce stable, dry electrodes suitable for electrochemical operation.

The assembled CDI unit was then integrated into a closed loop testing system consisting of a peristaltic pump, a solution reservoir, and a DC power supply. The pump continuously circulated P- and F-contaminated water through the CDI cell. Upon application of voltage across the electrodes, ions were electrostatically attracted and adsorbed onto the oppositely charged electrodes. Initially, ion removal occurred rapidly due to the high surface availability. As the adsorption sites approached saturation, the removal rate declined and eventually plateaued, indicating electrochemical equilibrium.[17]

Once saturation was reached, the polarity of the DC supply was reversed to initiate the desorption phase, releasing the adsorbed ions and regenerating the electrodes. This cyclic process was repeated multiple times, demonstrating the reusability and stability of the CDI system for water purification applications.

3.5. Hazards and Safety Precautions. This experiment involved multiple types of laboratory hazards, particularly those associated with electrical equipment and hazardous chemicals. Students followed strict safety protocols at all times. Personal protective equipment, such as lab coats, gloves, face masks, and protective goggles, was worn throughout the experiment.

High-temperature devices such as tube furnaces and drying ovens were operated only by experienced students or under supervision. Chemicals were carefully measured and handled to avoid spills or overexposure. All working areas were kept clean and organized, and chemical waste was disposed of following laboratory regulations.

Several chemicals used in the experiment pose significant health risks:

$MgCl_2$ and $AlCl_3$:Cause skin and eye irritation; inhalation may result in respiratory discomfort.

KH_2PO_4 and NaF: May cause skin and eye irritation; excessive exposure can lead to respiratory distress, chest pain, or nausea.

HNO_3 and NaOH:Highly corrosive; can cause permanent skin burns and lung damage if inhaled.

Acetone and PVDF:Lower toxicity but flammable; require careful handling to prevent fire or skin irritation.

All students were briefed on the Material Safety Data Sheets for each chemical. Emergency protocols, such as eyewash and spill response procedures, were also reviewed. The overall focus was to foster a culture of laboratory safety, chemical hygiene, and responsible experimentation.

4. RESULTS AND DISCUSSION

The following characterization results are derived from the Mg−Al−BC sample fabricated by one of the student groups. These results are obtained through strict adherence to standardized experimental procedures and reflect the initial stages of hands-on learning. Emphasis was placed not only on the experimental outcomes but also on the educational value of understanding the synthesis and evaluation process.

All experimental steps were carried out under the guidance of a senior student and the course instructor to ensure consistency and safety. By the end of the procedure, students had developed a comprehensive understanding of the workflow, and several demonstrated the ability to independently replicate key steps. A comparative analysis of the pre- and postexperiment evaluation scores is presented in a later section to underscore the learning impact.

4.1. Characterization of Mg−Al−BC and Mg−Al−BC−F/P Samples. Figure 3 shows the FESEM and EDS analyses

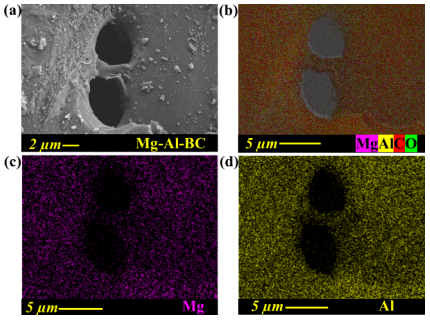

Figure 3. (a) FESEM image of Mg−Al−BC; (b) EDS elemental mapping of Mg and Al; (c) relative density of Mg; (d) relative density of Al in the doped biochar.

of the synthesized Mg−Al−BC sample. Figure 3a reveals a highly porous structure, which can be attributed to activation with $MgCl_2$ and $AlCl_3$. The resulting semicircular pore morphology is consistent with previous findings suggesting that lower activation temperatures promote uneven and irregular pore formation.[18] This microstructure enhances the material's adsorption capacity relative to pristine biochar. Figure 3b−d confirms the successful incorporation of Mg and Al into the biochar matrix via EDS mapping, demonstrating uniform distribution across the sample surface.

Figure 4a shows the surface structure of the Mg−Al−BC−F/P sample after the CDI process. The roughened surface, further enhanced by Mg and Al doping, facilitates the adsorption of the ions. Figure 4b−d shows elemental mapping that confirms the adsorption of the F and P ions. The elemental composition report showed an incorporation of 6.25% F and 0.72% P ion content.

https://doi.org/10.1021/acsomega.5c05966
ACS Omega XXXX, XXX, XXX−XXX

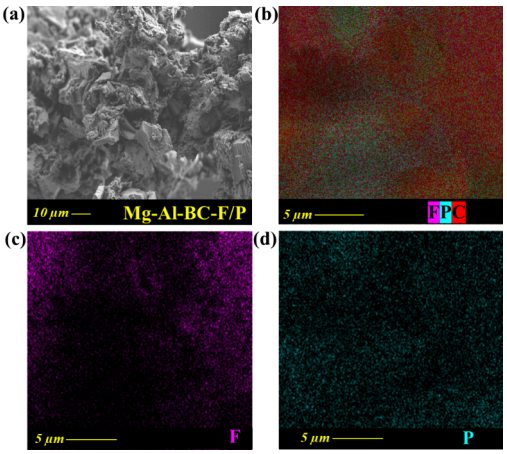

Figure 4. (a) FESEM image of Mg−Al−BC−F/P after the CDI experiment; (b) EDS mapping showing F and P; (c) F ion density; (d) P ion density.

Figure 5 shows the XRD patterns of the Mg−Al−BC and Mg−Al−BC−F/P samples. For the Mg−Al−BC sample, the diffraction peak at 24.3° corresponds to the (012) plane of amorphous Al_2O_3 (JCPDS 10−0173), while the peak at 42.97° confirms the presence of MgO. These features demonstrate successful incorporation of Al and Mg into the carbon matrix. The XRD result of the Mg−Al−BC−F/P sample shows diminished MgO peaks and a shift in Al_2O_3 diffraction, suggesting active participation of these oxides in the ion adsorption process.[19]

FTIR analysis in Figure 5b confirms the functional groups responsible for adsorption. In Mg−Al−BC, a broad absorption at 3406 cm^{-1} and a peak at 1578 cm^{-1} signify O−H stretching and bending of the −H, indicating hydroxyl groups and hydrogen bonding. Peaks at 2926 and 2855 cm^{-1} correspond to C−H stretching, while the C−O stretch appears at 1110 cm^{-1}. The COO^- vibration at 1389 cm^{-1} and metal−oxygen bond at 544 cm^{-1} further confirm the presence of Mg−O and Al−O functionalities, which are crucial for the adsorption of P and F ions.

Figure 6a shows the full XPS survey spectra as well as the deconvoluted peaks in Figure 6b, with Figure 6e highlighting the presence of C 1s (284.8 eV) and O 1s (533.1 eV). Postadsorption, the Mg−Al−BC−F/P sample shows additional peaks at 120.34 eV (P 2p) (Figure 6h) and 687.9 eV (F 1s) (Figure 6i), confirming the adsorption of P and F ions. Peaks at 65.4 eV (Figure 6d) and 1304.4 eV (Figure 6f) as well as Figure 6g validate the successful doping of Al and Mg, respectively. A comparison between Figure 6c,f indicates that Mg primarily exists as MgO in Mg−Al−BC because of the Mg 2p orbital energy shown in the figures, which later interacts with targeted ions by enhancing the adsorption ability of the material. The chemical reactions involved in the ion exchange and surface complexation processes are elaborated in subsequent equations, highlighting the physicochemical interactions governing the CDI performance. Equation 3 shows the formation of $MgHPO_4$ due to the chemical reaction between $Mg(OH)_2$ and HPO_4^{2-}. This denotes the direct adsorption of P from water by the Mg atoms present in the biochar electrodes. This compound remains as surface sedimentation on the electrode surface.[20] On the other hand, Al also contributes to the adsorption of both P and F^- ions. The mechanism can be attributed to Al−O formation, as shown in Figure 6g. This compound reduces the electrostatic repulsion between the Al and P ions present on the biochar as well as the P present in the solution. This phenomenon enhances the adsorption of P through Al in the solution. An intermediate compound may build up during the process. The compound is ($O-Al-O-H_2PO_3^-$), with the first oxygen atom bonded to the carbon atom in the biochar material. Both of these atoms, while present on the biochar surface, control the pH of the environment, which is one of the most important factors for P ion adsorption from wastewater.[21] A detailed explanation can be found in Figure 13, which presents all of the chemical compounds and their possible reactions.

$$MgO + H_2O \rightarrow Mg(OH)_2 \quad (1)$$

$$Mg(OH)_2 + 2H_2PO_4^- \rightarrow Mg(H_2PO_4)_2 + 2OH^- \quad (2)$$

$$Mg(OH)_2 + HPO_4^{2-} \rightarrow MgHPO_4 + 2OH^- \quad (3)$$

Nitrogen adsorption−desorption isotherms in Figure 7 provide information on the surface area and porosity. The Mg−Al−BC sample exhibits a type IV isotherm with a prominent hysteresis loop, confirming a mesoporous structure. BET surface area was calculated to be 350.74 m^2/g, with a pore volume of 0.469 cm^3/g. After adsorption (Mg−Al−BC−F/P), the surface area decreased to 288 m^2/g, and the pore volume slightly increased to 0.53 cm^3/g, indicating successful ion

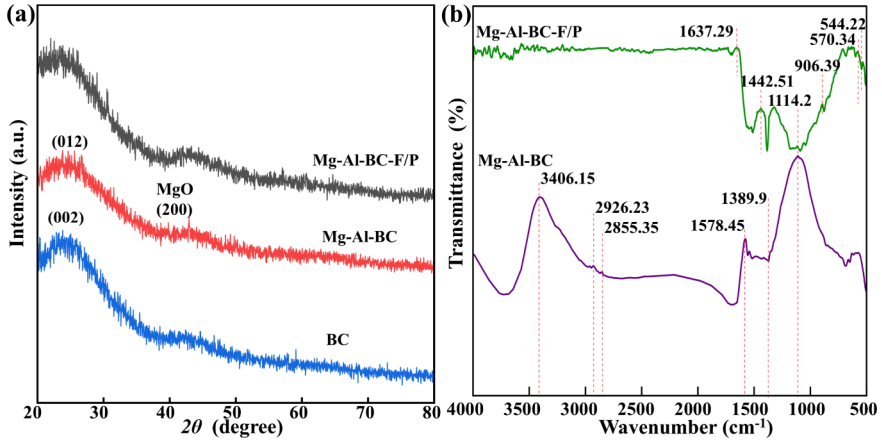

Figure 5. (a) XRD patterns and (b) FTIR of the Mg−Al−BC and Mg−Al−BC−F/P samples.

https://doi.org/10.1021/acsomega.5c05966
ACS Omega XXXX, XXX, XXX−XXX

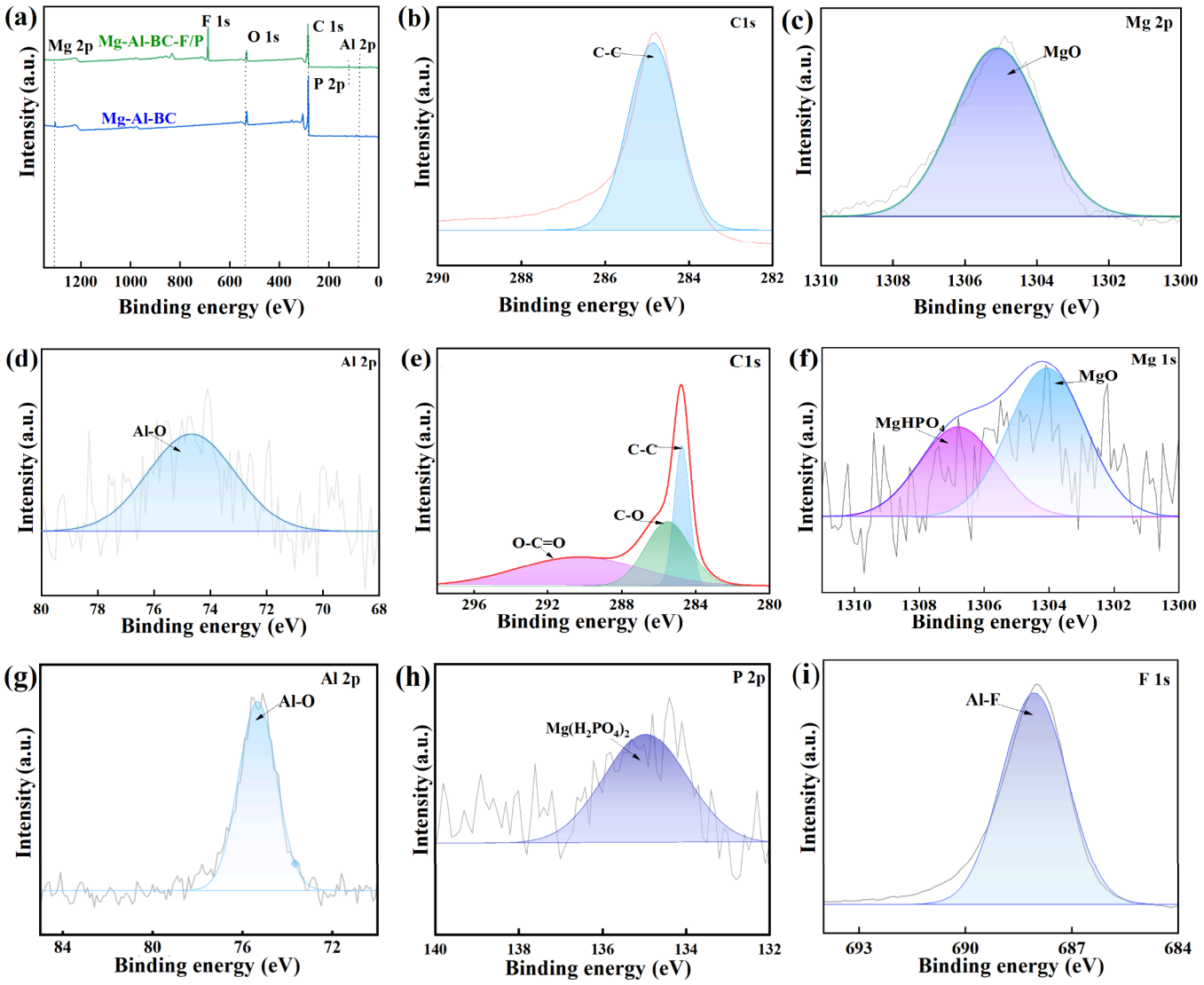

Figure 6. (a) XPS full spectra of Mg−Al−BC and Mg−Al−BC−F/P; (b−d) C 1s, Mg 2p, and Al 2p of Mg−Al−BC; (e−i) C 1s, Mg 2p, Al 2p, P 2p, and F 1s of Mg−Al−BC−F/P.

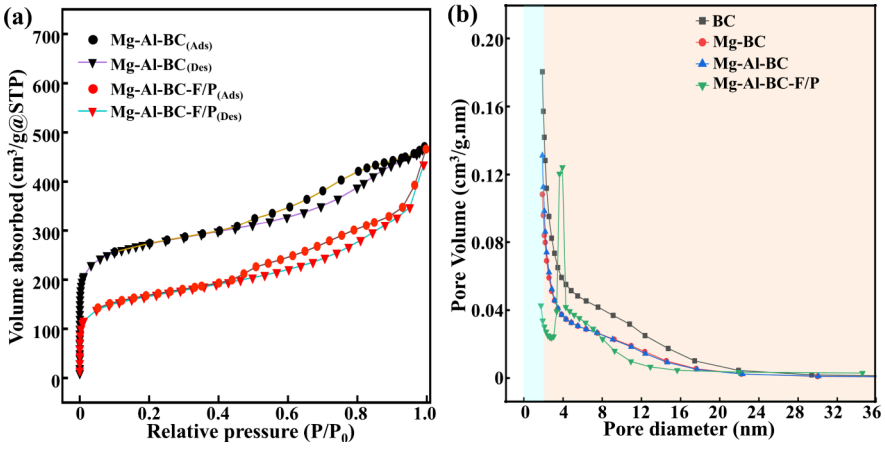

Figure 7. (a) N_2 adsorption−desorption isotherms; (b) BJH pore diameter distributions of Mg−Al−BC and Mg−Al−BC−F/P.

capture and partial pore blockage. The pore size distribution based on Barrett−Joyner−Halenda characterization (Figure 7b) shows dominant mesopores (2−50 nm), which are essential for efficient ion diffusion and adsorption. A notable drop in volume toward the macropore region further confirms the controlled porosity.

Figure 8 presents the electrochemical performance results of the developed electrode samples, focusing on cyclic voltam-

https://doi.org/10.1021/acsomega.5c05966
ACS Omega XXXX, XXX, XXX−XXX

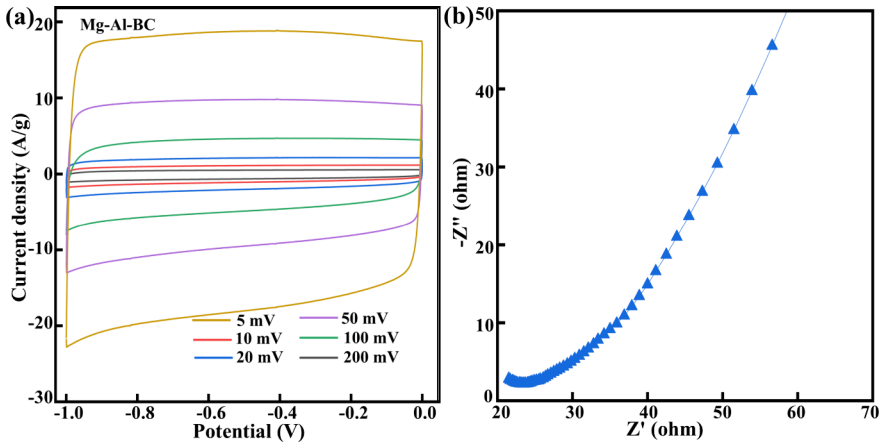

Figure 8. Cyclic volumetric results of the samples of (a) Mg−Al−BC; (b) EIS spectrum of Mg−Al−BC.

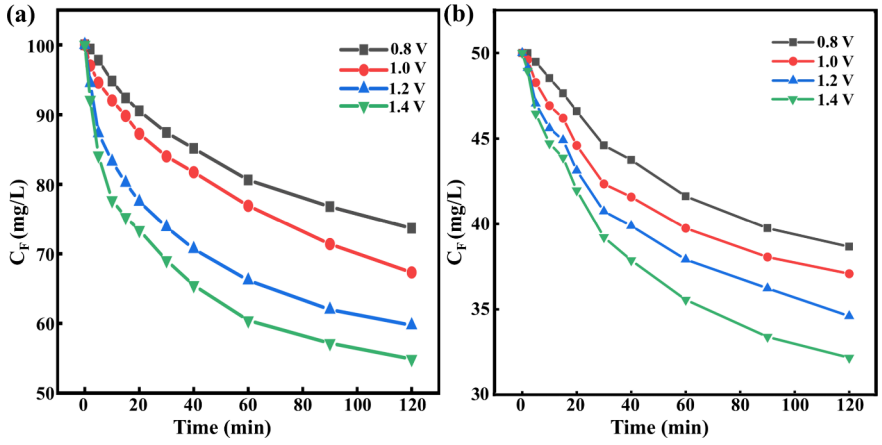

Figure 9. Effect of (a) operating voltage for CDI performance of soluble phosphorus; (b) operating voltage for CDI performance of F ions.

metry (CV) to assess the specific capacitance. A larger enclosed area within the CV (Figure 8a) curve indicates higher capacitance, while the shape of the curve provides insight into the type of capacitance exhibited, either electrical double-layer capacitance (EDLC) or pseudocapacitance. A predominantly rectangular shape in the central region suggests EDLC behavior, whereas deviations from this shape point to pseudocapacitive contributions. The Mg−Al−BC sample exhibits a specific capacitance of 114.06 F g^{-1} at a current density of 0.5 A g^{-1} (**S4**), which is superior to that of the Mg−BC electrode. Reactivation with Al_2O_3 alters the surface morphology, as confirmed by the SEM image in Figure 3d, resulting in a rougher texture that can accommodate more ion accumulation. Although a slight reduction in the specific surface area might decrease EDLC contributions, the incorporation of Mg and Al introduces additional electrochemically active sites, thereby enhancing the pseudocapacitive response and compensating for the loss in EDLC behavior. Structural analyses using XRD and FTIR reveal modifications in the crystalline and pore structures of Mg−Al−BC, supporting this enhancement. Additionally, the CV curves remained stable across different current densities, suggesting a consistent capacitance behavior. The Nyquist plot in Figure 8b features an arc near the origin, indicating low charge transfer resistance and efficient ion migration. The slope of the low-frequency region is less than 45°, reflecting the presence of both micropores and mesopores, which aid in ion transport and storage.

4.2. Effect of Operational Parameters on CDI Performance. *4.2.1. Operating Voltage.* The experimental setup used to evaluate the influence of operating voltage is shown in Figure S3. Figure 9 demonstrates the critical role of the applied voltage on the CDI performance of Mg−Al−BC electrodes. The adsorption efficiency of both P and F ions increases with voltage, peaking at 1.4 V. However, while 1.4 V offers the highest adsorption rate, it also leads to unwanted side effects such as gas bubble formation due to enhanced electrochemical activity. These bubbles are a result of Faradaic side reactions at higher voltages, which can damage the electrode by causing localized corrosion and uneven biochar detachment from the titanium substrate. Thus, although 1.4 V shows slightly better ion removal efficiency, 1.2 V is considered the optimal voltage due to its balance between performance and electrode stability. Specifically, the adsorption efficiency for P ions is measured at 26.4%, 32.69%, 40.26%, and 45.26% for 0.8 1.0, 1.2, and 1.4 V, respectively, in Figure 9a. For F ions, the corresponding values are 22.68%, 25.84%, 30.8%, and 35.68%, as depicted in Figure 9b. These results confirm that the Mg−Al−BC electrodes are effectively integrated into the CDI system, enabling a gradual reduction in ion concentration over time through increased electrostatic attraction under optimal voltage.[22]

4.2.2. pH Value. Figure 10 illustrates the variation in P and F ion adsorption as a function of solution pH. The highest adsorption efficiency is observed at a mildly acidic pH of around 5. At lower pH values, the surface of the biochar

https://doi.org/10.1021/acsomega.5c05966
ACS Omega XXXX, XXX, XXX−XXX

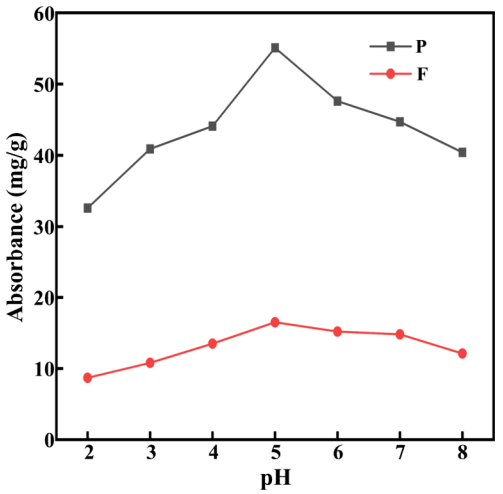

Figure 10. Effect of pH on P and F ion adsorption.

becomes protonated, acquiring a positive surface charge. This enhances the electrostatic attraction of negatively charged anions like P and F.[23] As the pH increases beyond 5, the surface charge transitions to negative, which induces repulsive interactions with anionic species, thus reducing adsorption efficiency. Furthermore, pH fluctuations during CDI can be attributed to several mechanisms: (a) asymmetric migration of anions and cations with different mobilities, (b) ion exchange and redox reactions within the electrode surface, and (c) Faradaic reactions that cause the most significant changes in pH.[24] The observed increase in pH from 5 to 8 under 1.2 V potential suggests the occurrence of oxygen reduction and carbon oxidation reactions, both of which are typical Faradaic processes. Additionally, non-Faradaic effects such as H^+/OH^- ion migration and surface complexation within micropores may also contribute to these fluctuations.[25] Therefore, maintaining an optimal pH of 4−5 is crucial for maximizing CDI performance in wastewater treatment.[26]

4.2.3. Feed Flow Rate. Figure 11 shows the variation in F (Figure 11a) and P (Figure 11b) ion adsorption at different flow rates ranging from 20 to 80 mL·min^{-1}. Maximum adsorption is observed at a flow rate of 50 mL·min^{-1}. While increasing the flow rate generally improves ion transport, excessively high rates at 80 mL·min^{-1} reduced the adsorption efficiency due to an insufficient contact time between the ions and the porous surface. This outcome can be linked to the structural characteristics of Mg−Al−BC, which is rich in mesopores that favor fast ion mobility.[27] However, for optimal retention of ions, a balance is needed between the flow speed and pore size distribution. Higher mesoporosity leads to rapid ion passage, reducing the probability of retention unless supplemented with micropores for better entrapment.[28] Therefore, a flow rate of 50 mL·min^{-1} offers an ideal balance between adsorption capacity and operational efficiency.

4.3. CDI Performance Analysis. The cyclic stability of Mg−Al−BC electrodes has been assessed over 16 consecutive adsorption−desorption cycles, as shown in Figure 12. These tests were performed at an applied voltage of 1.2 V, a flow rate of 50 mL·min^{-1}, and a 3 mm electrode spacing. After multiple cycles, the electrode retains 94.2% of its initial electrosorption performance (salt adsorption capacity), indicating excellent structural integrity and regeneration capability. The slight decline in performance over the cycles confirms the electrode's durability and reusability, which are crucial factors for practical implementation in wastewater treatment.

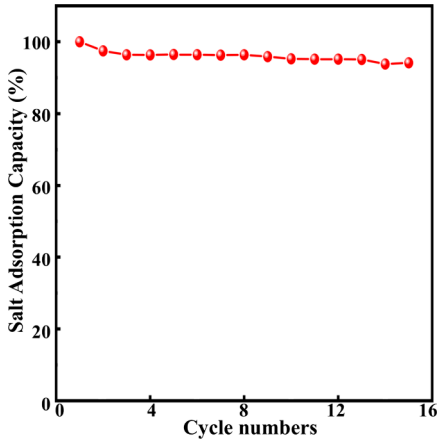

Figure 12. Long-term cycle ability of the Mg−Al−BC electrode.

The energy consumption was calculated based on the total charge passed during the adsorption process. The consumption test was conducted under standard laboratory conditions. The experiment was performed at room temperature; pH was maintained at 5 and 1.2 V was applied to ensure optimum ion adsorption. The initial concentrations of P and F ions were

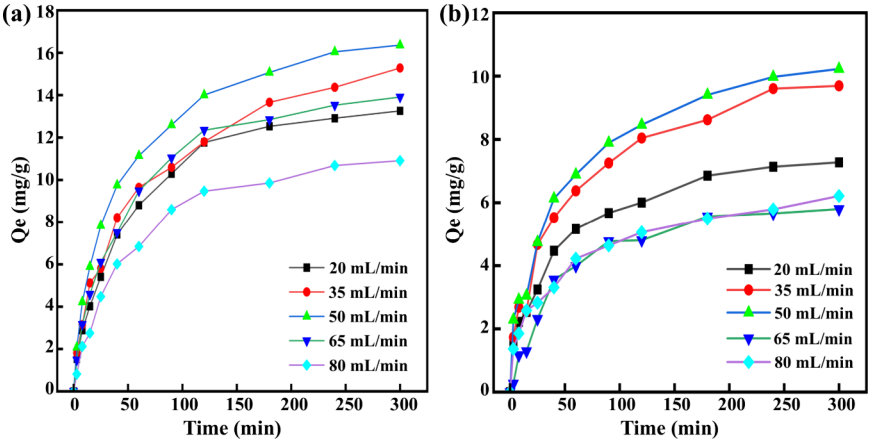

Figure 11. Rate of flow according to time and representation of (a) F and (b) P ion adsorption.

https://doi.org/10.1021/acsomega.5c05966
ACS Omega XXXX, XXX, XXX−XXX

0.031% and 0.007%, respectively. The energy input was determined using the following equation:

$$E_{in} = \int_0^t IV\,dt \tag{4}$$

where I is the instantaneous current (A), V is the applied voltage (1.2 V), and t is the charging time (s).

The calculated specific energy consumption is 0.000306 kWh·m^{-3}. This indicates higher performance based on low power input, which can be attributed to the biochar surface structure, which is very favorable for ion adsorption. The Mg and Al have developed the wettability and ion adsorption capacity of the prepared sample. The stability of the materials depends on their cycling ability as well as the amount of energy consumed during real-time tests. This excellent cyclic stability and low energy consumption reflect strong structural integrity and regeneration capability. The low specific energy consumption further highlights the material's efficiency, attributed to the enhanced surface properties imparted by Mg and Al doping. As the deionization process continues, the stability of the electrode gradually decreases. Therefore, parameters were controlled to maintain consistent overall adsorption performance by the electrode materials from the beginning to the end of the tests.

Figure 13 depicts the overall adsorption mechanism and the presence of P ions in various compound forms. The F ions can also remain in a manner similar to that of the P ions. The schematic illustrates different compounds interacting with the doped metal ions present on the surface of the biochar materials. It can be observed that P-containing ionic groups are deposited on the material's surface through different chemical reactions. These remain as sediments, and during the desorption process, they are released as effluents from the biochar materials.

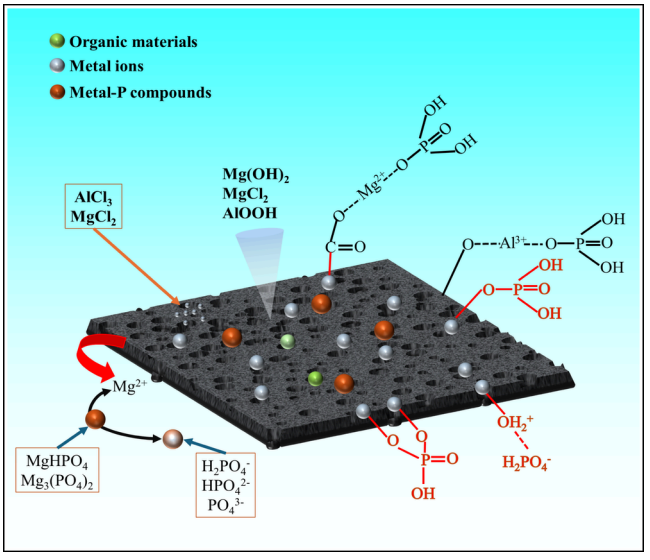

Figure 13. Overall ion adsorption mechanism in wastewater.

5. STUDENTS' EVALUATION

Before the experiment, the students were given three lectures on basic steps and were handed out some research summaries. On a scale of 5, all 15 students were evaluated according to their level of understanding. Here, 1 indicates no understanding, and 5 indicates complete understanding. Table 1 presents all of the evaluations.

Table 1. Evaluation of Students after Discussing the CDI Process with Them

questions	1	2	3	4	5
Understand the capacitive deionization process					15
Understand how the biochar is prepared					15
Can activate the biochar with different activators	7	1	2	1	4
How the activator is chosen is clear to me	2	3	3	5	2
Can describe the electrochemical process of the electrode	8	3		1	3
Can describe the whole process from the synthesis of biochar to the deionization capacity testing	1		8	5	1

They were evaluated after the experiment on their understanding of the process (Table 2). The evaluation is presented in the table below. Here, the students showed remarkable progress in understanding after completing the experiment.

Table 2. Evaluation of Students after the CDI Experiment Was Complete

point of understanding	number of students able to demonstrate
Understand the capacitive deionization process	15
Understand how the biochar is prepared	15
Can activate the biochar with different activators	12
How the activator is chosen is clear to me	14
Can describe the electrochemical process of the electrode	15
Can describe the whole process from the synthesis of biochar to the deionization efficiency testing	12

CONCLUSIONS

This study explores a student-driven capacitive deionization (CDI) system using coconut shell-derived biochar codoped with $MgCl_2$ and $AlCl_3$ for phosphate and fluoride removal from water. The doped electrodes exhibited improved adsorption capacity, 94.2% cyclic stability, and a low energy consumption of 0.000306 kWh·m^{-3} at an optimal flow rate of 50 mL·min^{-1}, showing strong applicability for real-world wastewater treatment. Around 80% of participating undergraduate students, primarily from materials science and chemical engineering, demonstrated the ability to independently synthesize electrodes, conduct electrochemical testing, and analyze data using tools like Microsoft Excel and OriginPro. The experiment significantly enhanced their understanding of electrochemical systems, sustainable materials, and water treatment technologies. This project serves as a practical model for integrating environmental challenges into engineering education while fostering self-reliance, critical thinking, and technical competence.

ASSOCIATED CONTENT

Data Availability Statement

Data used is available throughout the manuscript text.

Supporting Information

The Supporting Information is available free of charge at https://pubs.acs.org/doi/10.1021/acsomega.5c05966.

https://doi.org/10.1021/acsomega.5c05966
ACS Omega XXXX, XXX, XXX−XXX

Instructor's notes and student's handout (PDF)

AUTHOR INFORMATION

Corresponding Authors

Sheikh Tamjidur Rahman − *Hubei Key Laboratory of Plasma Chemistry and Advanced Materials, Wuhan Institute of Technology, Wuhan 430073, China;* orcid.org/0000-0002-7213-7300; Email: s.tamjidur@gmail.com

Qirui Wu − *Wuhan NARI Limited Liability Company, State Grid Electric Power Research Institute, Wuhan 430074, China*; Phone: + 86-027-87195661; Email: d202080416@126.com; Fax: + 86-027-87195661

Authors

Geming Wang − *Hubei Key Laboratory of Plasma Chemistry and Advanced Materials, Wuhan Institute of Technology, Wuhan 430073, China*

Shiyu Zhou − *School of Arts and Design, Wuhan Technology and Business University, Wuhan 430070, China*

Ziheng Yang − *Hubei Key Laboratory of Plasma Chemistry and Advanced Materials, Wuhan Institute of Technology, Wuhan 430073, China*

Dingdu Chen − *Hubei Key Laboratory of Plasma Chemistry and Advanced Materials, Wuhan Institute of Technology, Wuhan 430073, China*

Hongyang Zhao − *Hubei Key Laboratory of Plasma Chemistry and Advanced Materials, Wuhan Institute of Technology, Wuhan 430073, China;* orcid.org/0000-0003-2731-7633

Zhe Chen − *Hubei Key Laboratory of Plasma Chemistry and Advanced Materials, Wuhan Institute of Technology, Wuhan 430073, China*

Shuangfeng Hu − *Hubei Key Laboratory of Plasma Chemistry and Advanced Materials, Wuhan Institute of Technology, Wuhan 430073, China*

Complete contact information is available at: https://pubs.acs.org/10.1021/acsomega.5c05966

Author Contributions

#G.W., S.Z., and Z.Y. contributed equally to this work.

Author Contributions

G.W. − Data curation; Writing − original draft. S.Z. − Data curation; Writing − original draft. Z.Y. − Data curation; Writing − original draft. D.C. − Resources; Software. H.Z. − Formal analysis; Funding acquisition. Z.C. − Formal analysis. S.H. − Formal analysis. S.T.R. − Methodology; Supervision; Writing − review and editing. Q.W. − Formal analysis; Supervision.

Notes

The authors declare no competing financial interest.

ACKNOWLEDGMENTS

Financial support from the teaching research project of Wuhan Institute of Technology, "Exploration of OBE Training Model for Outstanding Engineering Talents in Materials for Local Engineering Colleges" (Grants No.: X2023015).

REFERENCES

(1) Qin, X.; Cao, y.; Guan, H.; Hu, Q.; Liu, Z.; Xu, J.; Hu, B.; Zhang, Z.; Luo, R. Resource utilization and development of phosphogypsum-based materials in civil engineering. *J. Clean Prod* **2023**, *387*, No. 135858.

(2) Wei, Z.; Deng, Z. Research hotspots and trends of comprehensive utilization of phosphogypsum: Bibliometric analysis. *J. Environ. Radioact* **2022**, *242*, No. 106778.

(3) Fan, Xuyang; Zhou; Chenyu Xiao; Tingting Wang; Haoran Wu; Hanjun Li; Zhongjun Pan; Zhiquan Zhou; Hong. Optimization of wet-process phosphoric acid for high-quality phosphogypsum. *Physicochem Probl Miner Process* **2024**, *60* (5), No. 192938.

(4) Ennaciri, Y.; Bettach, M. The chemical behavior of the different impurities present in Phosphogypsum: a review. *Phosphorus Sulfur Silicon Relat Elem* **2024**, *199*, 129−48.

(5) Li, Keyao; Shi; Chunyu Zeng; Yanqi Huang; Lingyun Chen; Bo Liu; Cheng Bao; Shenxu Yang; Siyuan. A high-efficiency purification method of waste phosphogypsum via hydrodynamic cavitation pretreatment and froth flotation. *J. Clean Prod* **2025**, *512*, No. 145685.

(6) Kalfa, A.; Shapira, B.; Shopin, A.; Cohen, I.; Avraham, E.; Aurbach, D. Capacitive deionization for wastewater treatment: Opportunities and challenges. *Chemosphere* **2020**, *241*, No. 125003.

(7) Ji H; Lee H-S; hyun Moon J; Thu K; Kim Y-D; Jeon W-J. Experimental and theoretical evaluation of a novel hybrid multi-effect adsorption desalination process. *Sep Purif Technol.* **2025**, *361*, No. 131522.

(8) Chang, Zhen Hong; Sum, Jing Yao; Lau, Woei Jye; Ang, Wei Lun; Teow, Yeit Haan; Ooi, Boon Seng; Yeap, Swee Pin Current State-of-the-Art of Non-Reverse Osmosis-Like Forward Osmosis Technology. *J. Membr. Sci.* **2024**, *711*, No. 123209.

(9) Sharshir, S. W.; Elsayad, M. M.; Ismail, M.; Kandeal, A. W. An innovative multi-stage flash distillation unit integrated with evacuate tubes water heater and water mists: A (4E/2S) estimation. *Energy Convers Manag* **2025**, *327*, No. 119548.

(10) Elawadi, G. A. Low-Energy Desalination Techniques, Development of Capacitive Deionization Systems, and Utilization of Activated Carbon. *Materials (Basel)* **2024**, *17*, 5130.

(11) Wang, Geming; Chen, Dingdu; Yang, Ziheng; Liao, Shilu; Tamjidur; Rahman Sheikh Hu; Shuangfeng Wu; Qirui Zhang; Weixin. Effectiveness of capacitive deionization for the removal of soluble phosphorus and fluoride with a Mg/Al co-doped porous biochar electrode during the process of water-washing of phosphogypsum. *Desalination* **2025**, *602*, No. 118640.

(12) Ge, S.; Zhao, S.; Wang, L.; Zhao, Z.; Wang, S.; Tian, C. Exploring adsorption capacity and mechanisms involved in cadmium removal from aqueous solutions by biochar derived from euhalophyte. *Sci. Rep* **2024**, *14*, 450.

(13) Nam, Deukhyeon; Moon, Joon Ha; Jin, Youngho; Seong, Honggyu; Choi, Bo Eun; Na, Chan Woong; Kang, Yun Chan; Myung, Yoon; Choi, Jaewon Exploring enhanced capacity in lithium-ion battery anodes: Synthesis and electrochemical evaluation of Zn2GeO4 encapsulated in porous carbon balls via carbonization. *J. Energy Storage* **2025**, *107*, No. 114858.

(14) Chen, Y.-W.; Chen, J.-F.; Lin, C.-H.; Hou, C.-H. Integrating a supercapacitor with capacitive deionization for direct energy recovery from the desalination of brackish water. *Appl. Energy* **2019**, *252*, No. 113417.

(15) Hu, Yongsheng; Hu, Bin; Ge, Yuanxin; Nie, Pengfei; Yang, Jianmao; Huang, Manhong; Liu, Jianyun In-situ synthesis of UiO-66-NH2 on porous carbon nanofibers for high performance defluoridation by capacitive deionization. *Colloids Surfaces A Physicochem Eng. Asp* **2022**, *646*, No. 129020.

(16) Liu, X.; He, X.; Dang, Y.; Li, X.; Yang, J.; Shi, W. Solidification and removal of impurities from phosphogypsum for road applications: a review. *Environ. Chem. Lett.* **2025**, *23*, 1111−43.

(17) Ippolito, James A.; Cui, Liqiang; Kammann, Claudia; Wrage-Mönnig, Nicole; Estavillo, Jose M.; Fuertes-Mendizabal, Teresa; Cayuela, Maria Luz; Sigua, Gilbert; Novak, Jeff; Spokas, Kurt; Borchard, Nils Feedstock choice, pyrolysis temperature and type influence biochar characteristics: a comprehensive meta-data analysis review. *Biochar* **2020**, *2*, 421−38.

(18) Ajien, A.; Idris, J.; Md Sofwan, N.; Husen, R.; Seli, H. Coconut shell and husk biochar: A review of production and activation

technology, economic, financial aspect and application. *Waste Manag Res. J. a Sustain Circ Econ* **2023**, *41*, 37−51.
(19) Yang, Kai; Li, Hang; Lin, Wenjun; Chen, Zihao; Peng, Shuangyi; Yu, Ke; Fang, Zhao Performance and mechanism of hierarchical porous Al2O3-MgO nanosheets for removing fluoride ions from industrial ZnSO4 solution. *Sep Purif Technol.* **2024**, *330*, No. 125255.
(20) Fang, Yueru; Ali, Amjad; Gao, Yuxi; Zhao, Peng; Li, Ronghua; Li, Xianxian; Liu, Junxi; Luo, Yuan; Peng, Yaru; Wang, Hailong; Liu, Hongbin; Zhang, Zengqiang; Pan, Junting Preparation and characterization of MgO hybrid biochar and its mechanism for high efficient recovery of phosphorus from aqueous media. *Biochar* **2022**, *4*, No. 0.
(21) Deng, Yu; Li, Min; Zhang, Zhan; Liu, Qiao; Jiang, Kele; Tian, Jingjie; Zhang, Ying; Ni, Fuquan Comparative study on characteristics and mechanism of phosphate adsorption on Mg/Al modified biochar. *J. Environ. Chem. Eng.* **2021**, *9*, No. 105079.
(22) Song, Ziteng; He, Jianzhou; Kouzehkanan, Seyed Morteza Taghavi; Oh, Tae-Sik; Olshansky, Yaniv; Duin, Evert C.; Carroll, Kenneth C.; Wang, Dengjun Enhanced sorption and destruction of PFAS by biochar-enabled advanced reduction process. *Chemosphere* **2024**, *363*, No. 142760.
(23) Lim, Jihun; Shin, Yong Uk; Hong, Seungkwan Enhanced Adsorption of Aqueous Pb(II) by Acidic Group-Modified Biochar Derived from Peanut Shells. *Water* **2024**, *16*, 1871.
(24) Zhang, X.; Chen, Y.; Wang, Q.; Sun, Y. Advances in heavy metal wastewater treatment with biochar adsorption. *Biofuels, Bioprod Biorefining* **2025**, 2751.
(25) Chu, Meile; Tian, Weijun; Zhao, Jing; Zhang, Dantong; Zou, Mengyuan; Lu, Zhiyang; Jiang, Junfeng Dual-activated biochar with a multichannel structure enhanced electrosorption capacity of capacitive deionization for sulfate removal from mining wastewater. *Desalination* **2023**, *556*, No. 116588.
(26) Wen, Y.; Huang, L.; Yan, J.; Feng, B. Efficient recovery of Nd(III) from aqueous solution by KMnO4-modified corn cob biochar. *J. Water Process Eng.* **2025**, *70*, No. 107010.
(27) Wang, Liuting; Zhou, Zhikang; Li, Xintong; Zeng, Lingyu; Xu, Wenjun; Ma, Yankun; Cai, Jinjun Enhanced removal of methylene blue from water by mesopore-dominant biochar from kelp: Kinetic, equilibrium and thermodynamic studies. *Colloids Surfaces A Physicochem Eng. Asp* **2024**, *688*, No. 133652.
(28) Bayar, Jalal; Ali, Nawab; Dong, Younsuk; Ahmad, Uzair; Anjum, Muhammad; Mehran Khan, Gul; Roz Zaib, Muhammad; Jalal, Arshad; Ali, Rovaid; Ali, Liaqat Biochar-based adsorption for heavy metal removal in water: a sustainable and cost-effective approach. *Environ. Geochem Health* **2024**, *46* (11), 428.

https://doi.org/10.1021/acsomega.5c05966
ACS Omega XXXX, XXX, XXX−XXX